18 Aug 2015

Raman Spectroscopy Applied to the Noninvasive Detection of Monosodium Urate Crystal Deposits

Declan J. Curran

Laurence Rubin

Mark R. Towler
Missouri University of Science and Technology, mtowler@mst.edu

Recommended Citation

Raman Spectroscopy Applied to the Noninvasive Detection of Monosodium Urate Crystal Deposits

LIBERTAS Academica
FREEDOM TO RESEARCH

Declan J. Curran[1], Laurence Rubin[2] and Mark R. Towler[1,3]

[1]Department of Mechanical and Industrial Engineering, Ryerson University, Toronto, ON, Canada. [2]Division of Rheumatology, St. Michael's Hospital, Faculty of Medicine, University of Toronto, Toronto, ON, Canada. [3]Department of Biomedical Engineering, University Malaya, Kuala Lumpur, Malaysia.

ABSTRACT: An off-the-shelf Raman Spectrometer (RS) was used to noninvasively determine the presence of monosodium urate (MSU) crystals on the metatarsophalangeal joint (MTPJ) of a single gout sufferer. The spectrum sourced from the clinically diagnosed gout sufferer was compared to that sourced from an age-matched healthy subject scanned using the same protocol. Minimal signal processing was conducted on both spectra. Peaks characteristic of MSU crystals were evident on the spectrum sourced from the gout sufferer and not on the spectrum from the healthy control.

KEYWORDS: Raman, monosodium, gout, MSU, spectroscopy

Introduction

Gout is the most common form of inflammatory arthritis, affecting around 3% of the population in both Europe and North America.[1] It is the result of hyperuricemia, which can cause deposition of monosodium urate (MSU) crystals in joints and other organs. When a critical level of crystal buildup is reached, the patient suffers acute arthritic attacks. Gout has related comorbidities of atherosclerosis, hypertension, obesity, and organ failure.[2] However, prognosis is excellent if diagnosed early and properly treated.[3]

The gold standard diagnostic technique for gout is needle aspiration of the synovial fluid (SF) from the affected joint and identification of MSU crystals in the SF by compensated polarized light microscopy.[4,5] This is an invasive, painful, and operator-dependent technique,[6–9] explaining why it is only used in 10% of cases.[2] Physicians more often make a diagnosis by a combination of clinical appearance of the joint and blood uric acid levels.[10] X-ray analysis (XRA), dual-energy computed tomography (DECT), and high-resolution ultrasound (HRUS) have also been used for gout diagnosis, and magnetic resonance imaging (MRI) has been evaluated as a diagnostic for research purposes.[11–21] Each of these techniques have their own inherent problems. XRA has poor prediction rates and is insensitive to early deposition.[11,12] MRI is superior to XRA at detecting gout,[13,14] but the appearance of gout on MRI is nonspecific[15] and contrast agents may be required.[13] Often DECT is unable to detect MSU in cartilage[16] and is less sensitive than aspiration.[17] In addition, DECT has significant cost implications, exposes the patient to radiation, and is available only to a few clinical units.[18] HRUS detects crystals *via* hyperechoic masses or linear bands in synovium of cartilage[19] and has improved sensitivity and cost savings over DECT.[18] However, it is successful only in chronic sufferers whose serum uric acid levels are elevated for over six months.[20,21] Additionally, an experienced sonographer is required and they can take at least 15 minutes to analyze each joint.[21]

Raman Spectroscopy (RS) may offer a noninvasive alternative to these techniques as a point-of-care gout diagnostic. RS is a technique whereby incident light can be absorbed or scattered by a material when the energy of an incident photon excites a molecule in the material being irradiated. A small portion of the scattered light is shifted in energy with respect to the source beam. Plotting light scattered against frequency results in a Raman spectrum, effectively a "fingerprint" of the material's molecular structure.[22] RS has clinical applicability for diagnosing cancer,[23] diabetes,[3,24] and Alzheimer's disease.[4,25] It has previously been reported that RS can detect MSU crystals in aspirated SF[26] but this process requires needle aspiration and subsequent enzyme digestion and microfiltration rendering it impractical for clinical purposes as it is more time consuming and no less invasive than the gold standard.

In this paper, we detail how RS can identify MSU crystals, noninvasively, around the first metatarsophalangeal joint (MTPJ) of a clinically diagnosed gout sufferer.

Materials and Methods

Device. The RS device used was a Sierra (Snowy Range Instruments). The Sierra has a 785 nm wavelength laser with a maximum power of 100 mW. This results in high spectral resolution of 4 cm^{-1} and a spectral range of 200–2000 cm^{-1}. The software used to interpret the Raman spectra was the inbuilt Snowy Range *Peak Software*™ (v3.08) and *GRAMS*™ (ThermoScientific) for post testing of the spectra. The system was configured to utilize Small Spot Sampling, giving the higher spectral resolution compared to the inbuilt patterned raster option.

Patients. Four clinically diagnosed gout sufferers were recruited through a trial conducted at St. Michael's Hospital (Toronto, Canada). All these patients were treated for gout, although only one patient was classed as having gout deposits. An age and gender matched healthy subject was selected and subjected to the same test protocol. The subject with gout is referred to as *Patient*, while the subject without gout is referred to as *Healthy*. The study was approved by the St. Michael's Hospital Ethics Board (REB# 14-902)), and all patients gave written consent as per the Declaration of Helsinki.

Figure 1 shows how the Sierra was aligned to the first MTPJ of the subject.

Laser testing protocol. The tests were conducted in a dark room to reduce interference from fluorescent lights. For both subjects, the RS was set to illuminate with an integration time of ten seconds, repeated automatically five times per selected point on the patients' body. This collected five Raman traces, each with an exposure time of ten seconds, with the average of these five traces per irradiated spot being calculated and stored as the final Raman spectrum seen in Figure 2. The exposure time was segmented into these ten-second blocks giving the skin a rest time. This segmentation also allowed flexibility, by removing completely or averaging, if any patient movement occurred during the ten-second burst. A number of spots around the MTPJ were also examined with the same procedure to ensure the detection of MSU deposits. This method of breaking up the exposure time was utilized to increase the chances of detecting MSU while keeping the laser exposure to the skin to a minimum.

Signal analysis and peak identification. Subjects were scanned without the RS reference signal being removed in real-time, meaning that the Raman signal contains contributions from both the RS device itself and the subject in question. This was intentional and assured that any contribution to spectra from MSU peaks were not removed by signal processing. However, background fluorescence was removed using the built-in *Peak Software* peak clean option, which pulled the measured spectra down to a baseline. GRAMS software was used to overlay the spectra to allow a direct comparison of peak wave numbers and the peak relative intensities between the *Healthy* and *Patient* spectra. For presentation purposes for this paper, the Raman spectra have been plotted against as a scaled intensity (0–1) on the *y*-axis. The MSU peaks have

Figure 1. Snowy Range Sierra RS underside lens port aligned against the patient's MTP joint.

been classified into three categories indicating their comparative parameters (Figs. 2 and 3):

- A square over the peak indicates the presence of a peak on both the *Healthy* and *Patient* spectra with comparable intensities between these peaks.
- A star indicates the presence of a peak on both the *Healthy* and *Patient* spectra where the relative peak intensity of the *Patient* spectrum is visually higher than that on the *Healthy* spectrum.
- An arrow indicates that there is no overlap between peaks of both spectra, ie, peaks present in the *Patient* spectrum have no comparable peak in the *Healthy* spectrum.

Results

Figure 2 compares the Raman spectra of the *Healthy* and *Patient* subjects. Both spectra contain contributions from both the device itself, skin and any other subcutaneous biological tissue that the laser contacts.

Initially, without comparing to the *Healthy* Raman trace, the *Patient* spectrum has 16 peaks that could be identified as classic MSU peaks, as reported in a study by Kodati et al.[27] (Fig. 3). When comparing to the *Healthy* Raman spectrum, these peaks are broken into three sections, four of these peaks (identified by the arrows) do not have comparative peaks in the *Healthy* spectrum; their wave numbers coexist with low-level noise at the equivalent wave number in the *Healthy* spectrum.
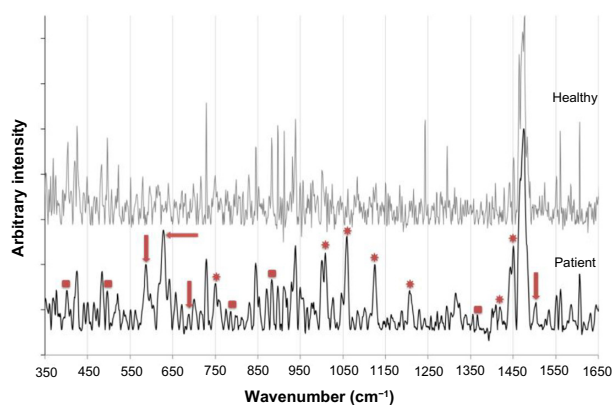
Figure 2. Trace from *Healthy* and *Patient* subjects.
Notes: Square = peak overlap with comparable intensities; star = peak overlap where intensity from the *Patient* spectrum is larger; arrow = no peak overlap between traces (ie, peak not in *Healthy* subject because of intensities being at a level considered as baseline signal/noise).
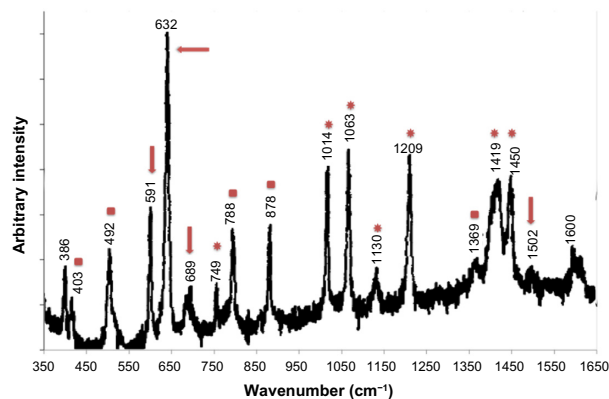

Figure 3. Raman spectrum of MSU taken from Kodati et al.[27] and edited by the incorporation of the same identifiers used in Figure 2.
Notes: Square = overlap with comparable intensities; star = overlap with patients intensities being much larger; arrow = no overlap between traces (ie, peak not in *Healthy* subject because of intensities being at a level considered baseline signal/noise).

Seven peaks (identified by the stars) have comparators at the same wave number in the *Healthy* spectrum; however when comparing intensities, the *Patient* peaks have a marked increase in intensity compared to their *Healthy* counterparts. Five peaks (identified by squares) indicate peaks in the *Patient* spectrum that have comparative peaks of similar intensity in the *Healthy* spectrum.

Discussion

These results indicate that MSU crystal deposits can be detected in clinically diagnosed gout sufferers by RS. Out of the 18 total MSU peaks identified by Kodati et al.[27], 16 were present in the Raman spectrum of the clinically diagnosed gout patient. MSU peaks 386 and 1600 cm^{-1} were not present in either the *Healthy* or *Patient* spectra. The four peaks related to MSU present in the *Patient* spectrum only were present at wave numbers 588, 628, 686, and 1503 cm^{-1} (Fig. 2), which translate as wave numbers 591, 632, 689, and 1502 cm^{-1} in biological grade MSU (arrows, Fig. 3). The authors hypothesize that the biologically deposited MSU crystals contain slightly different molecular bond energies, resulting in the slight shifts in the Raman peak wave numbers reported here. The different environmental conditions, such as pH and temperature, in which crystals are deposited in the body may result in changes in molecular bonding and packing of the MSU crystal in and around the MTPJ, which would also explain the peak shifts compared to the laboratory synthesized sodium urate trace in Figure 3.

The majority of the other peaks that identify MSU (Fig. 3) is present in both the *Healthy* and the *Patient* spectra (Fig. 2) and is indicated by both stars and squares (Fig. 2). These 12 peaks do have what seem like counterpart peaks with similar wave numbers in the *Healthy* spectrum. The peaks identified with a square cannot, at this stage, be identified as different to their *Healthy* spectrum counterparts; however, the intensities of the seven star identified peaks increase in

intensity compared to their *Healthy* peak counterparts. The Raman peaks of skin generally consists of the constituents of the stratum corneum with peaks existing at 855, 880, 1061, 1128, 1296, 1655, and 1747 cm^{-1}, as determined by Caspers et al.[28], as such the majority of these corresponding peaks in the *Healthy* spectrum is considered noise, with the exception of the 880, 1061, and 1128 cm^{-1}. These peaks are considered comparable to the MSU peaks of 878, 1063, and 1130 cm^{-1}. The 878 cm^{-1} MSU peak has been identified with a square, as such has been ignored in determining the presence of MSU crystals. Both the 1061 and 1128 cm^{-1} peaks have comparative peaks in the *Healthy* spectrum, which can be related to skin. However, the intensity of these peaks in the *Patient* spectrum compared to their healthy counterpart peaks implies that these peaks are most likely because of MSU. This is not the case for the other MSU peaks that are marked with a star; their comparative *Healthy* peaks are most likely noise as no Raman peaks at these wave numbers occur in skin.

Conclusion

The Sierra RS may have the ability to noninvasively identify MSU deposits at MTP joints. This preliminary study has shown that four Raman peaks (arrows) because of the MSU can be detected through the skin with no counterpart peaks associated with the *Healthy* control. Seven Raman peaks (stars) of MSU can be discerned in the *Patient* Raman spectrum; however, these peaks have corresponding peaks in the *Healthy* Raman spectrum. Two of these peaks have comparable Raman peaks with the known Raman peaks of skin; however, their intensity is greater than those in skin, implying that their origin is not skin. The *Healthy* peak counterpart of the other star identified MSU peak is considered noise. Five MSU peaks (squares) have counterpart peaks in the *Healthy* spectrum, and as such these peaks cannot be discerned from those generated in the Healthy spectrum, and as such they are ignored

and not used in the detection of MSU in this study. These preliminary results show that 10 Raman peaks (arrows and stars) can be used for the noninvasive identification of MSU deposits with minimal signal analysis.

Experimental Concerns

- The subjects were scanned without removing contributions from the RS background signal, ie, the portions of the spectrum that come from the internal optics of the RS. Incorporating an algorithm that can remove this needless contribution during real-time subject scanning should remove some of the noise from the spectra.

- Ergonomics of the machine influence analysis. The Sierra does not have an adjustable focal point meaning that the subjects had to be physically manipulated until the laser shone directly onto the MTPJ. This could be addressed by the incorporation of a focus wheel on the device, which would enable the operator to refocus the apparatus until they were confident that they were hitting the MTPJ. Additionally, most MSU deposits collect on the top of the MTPJ, not the side. However, the Sierra weighs 9 kg and so placing this device on the top of the MTPJ was not possible.

Author Contributions

Conceived and designed the experiments: DC, MT. Analyzed the data: DC, MT. Wrote the first draft of the manuscript: DC. Contributed to the writing of the manuscript: DC, MT, LR. Agree with manuscript results and conclusions: DC, MT, LR. Jointly developed the structure and arguments for the paper: DC, MT. Made critical revisions and approved final version: DC, MT, LR. All authors reviewed and approved of the final manuscript.

REFERENCES

1. Roddy E, Doherty M. Epidemiology of gout. *Arthritis Res Ther*. 2010;12(6):223.
2. Terkeltaub R, Edwards NL. Gout: Diagnosis and Management of Gouty Arthritis and Hyperuricemia. Professional Communications; 2011.
3. Medtrack. Medtrack Epidemiology Report – Gout; 2012.
4. McCarthy D, Hollander J. Identification of urate crystals in gouty synovial fluid. *Ann Intern Med*. 1961;54(3):452–60.
5. Lally EV, Zimmermann B, Ho G Jr, Kaplan SR. Urate-mediated inflammation in nodal osteoarthritis: clinical and roentgenographic correlations. *Arthritis Rheum*. 1989;32(1):86–90.
6. Schumacher HR, Sieck MS, Rothfuss S, et al. Reproducibility of synovial fluid analyses. a study among four laboratories. *Arthritis Rheum*. 1986;29(6):770–4.
7. Hasselbacher P. Variation in synovial fluid analysis by hospital laboratories. *Arthritis Rheum*. 1987;30(6):637–42.
8. Essen RV, Hölttä AMH. Quality control of the laboratory diagnosis of gout by synovial fluid microscopy. *Scand J Rheumatol*. 1990;19(3):232–4.
9. McGill NW, York HF. Reproducibility of synovial fluid examination for crystals. *Aust N Z J Med*. 1991;21(5):710–3.
10. Schlesinger N. Diagnosis of gout: clinical, laboratory, and radiologic findings. *Am J Manag Care*. 2005;11(15 suppl):S443–50.
11. Peh WC. Tophaceous gout. *Am J Orthop (Belle Mead NJ)*. 2001;30(8):665.
12. Buckley T. Radiologic features of gout. *Am Fam Physician*. 1996;54(4):1232–8.
13. Schumacher HR, Becker MA, Edwards NL, et al. Magnetic resonance imaging in the quantitative assessment of gouty tophi. *Int J Clin Pract*. 2006;60(4):408–14.
14. Schlesinger N. Diagnosis of gout. *Minerva Med*. 2007;98(6):759–67.
15. Dhanda S, Jagmohan P, Tian QS. A re-look at an old disease: a multimodality review on gout. *Clin Radiol*. 2011;66(10):984–92.
16. Huppertz A, Hermann K-GA, Diekhoff T, Wagner M, Hamm B, Schmidt WA. Systemic staging for urate crystal deposits with dual-energy CT and ultrasound in patients with suspected gout. *Rheumatol Int*. 2014;34(6):763–71.
17. Melzer R, Pauli C, Treumann T, Krauss B. Gout tophus detection – a comparison of dual-energy CT (DECT) and histology. *Semin Arthritis Rheum*. 2014;43(5):662–5.
18. Gruber M, Bodner G, Rath E, Supp G, Weber M, Schueller-Weidekamm C. Dual-energy computed tomography compared with ultrasound in the diagnosis of gout. *Rheumatology*. 2013;7:ket341.
19. Perez-Ruiz F, Dalbeth N, Urresola A, de Miguel E, Schlesinger N. Imaging of gout: findings and utility. *Arthritis Res Ther*. 2009;11(3):232.
20. Grassi W, Meenagh G, Pascual E, Filippucci E. "Crystal clear" – sonographic assessment of gout and calcium pyrophosphate deposition disease. *Semin Arthritis Rheum*. 2006;36(3):197–202.
21. Thiele RG, Schlesinger N. Diagnosis of gout by ultrasound. *Rheumatology*. 2007;46(7):1116–21.
22. Smith E, Dent G. *Modern Raman Spectroscopy: A Practical Approach*. John Wiley & Sons; 2005 [cited December 19, 2014]. Available from: http://books.google.ca/books?hl=en&lr=&id=PEkokAaO6I4C&oi=fnd&pg=PR5&dq=Modern=Raman=Spectroscopy&ots=JD2W1HHGSs&sig=f1Qmj0jEO2WMsfWaxYky2y8hpPg
23. Verisante. Available from: http://www.verisante.com
24. Suresh E. Diagnosis and management of gout: a rational approach. *Postgrad Med J*. 2005;81(959):572–9.
25. Zhu Y, Pandya BJ, Choi HK. Prevalence of gout and hyperuricemia in the US general population: the national health and nutrition examination survey 2007–2008. *Arthritis Rheum*. 2011;63(10):3136–41.
26. Li B, Yang S, Akkus OA. Customized Raman system for point-of-care detection of arthropathic crystals in the synovial fluid. *Analyst*. 2014;139(4):823–30.
27. Kodati VR, Tu AT, Turumin JL. Raman spectroscopic identification of uric-acid-type kidney stone. *Appl Spectrosc*. 1990;44(7):1134–6.
28. Caspers PJ, Lucassen GW, Wolthuis R, Bruining HA, Puppels GL. *In vitro* and *in vivo* Raman spectroscopy of human skin. *Biospectroscopy*. 1998;2:S31–9.